

Agent-Based Analysis of Electricity Contract Switching considering Multi-Dimensional Consumer Satisfaction and Social Influence

*Original*

Agent-Based Analysis of Electricity Contract Switching considering Multi-Dimensional Consumer Satisfaction and Social Influence / Chen, Jingsi; Yin, Jun; Meo, Michela; Huang, Tao. - In: ENERGY. - ISSN 0360-5442. - 351:(2026).  
[10.1016/j.energy.2026.140806]

*Availability:*

This version is available at: 11583/3009200 since: 2026-03-25T09:31:42Z

*Publisher:*

Elsevier

*Published*

DOI:10.1016/j.energy.2026.140806

*Terms of use:*

This article is made available under terms and conditions as specified in the corresponding bibliographic description in the repository

*Publisher copyright*

(Article begins on next page)

# REMOTE ASSESSMENT OF CARDIODYNAMIC CHANGES IN COMPETITIVE CYCLISTS DURING AN INCREMENTAL CYCLE-ERGOMETER TEST TO EXHAUSTION: A PILOT STUDY

Tocco F<sup>1,8</sup>, Manuello Bertetto A<sup>2</sup>, Velluzzi F<sup>1</sup>, Roux A<sup>2</sup>, Rosadelli S<sup>2</sup>, Fois A<sup>3</sup>, Deledda A<sup>1</sup>, Cappai EA<sup>1</sup>, Melis S<sup>1,4,8</sup>, Dell'Osa AH<sup>5</sup>, Cerina A<sup>6</sup>, Marcello R<sup>7</sup>, Concu A<sup>7,8</sup>

<sup>1</sup>Department of Medical Sciences and Public Health, University of Cagliari, Italy

<sup>2</sup>Department of Mechanical and Aerospace Engineering, Politecnico di Torino, Turin, Italy

<sup>3</sup>Nomadyca Ltd, Remote Biosignals Acquisition Unit, Mulago Hospital, Kampala, Uganda

<sup>4</sup>Sardinia's Schools Direction Office, Physical and Sports Education Unit, Ministry of Education and Merit, Cagliari, Italy

<sup>5</sup>Laboratorio de Electrónica Aplicada y Biomedicina, Universidad Nacional de Tierra del Fuego, Ushuaia, Argentina

<sup>6</sup>Acquaforte Thalasso & Spa Medical Team, Forte Village Resort, Santa Margherita di Pula, Cagliari, Italy

<sup>7</sup>AC Technologies Ltd, Bioimpedance Devices Manufacturing, Cagliari, Italy

<sup>8</sup>Sporting Life & Medicine Lab, Sardegna Ricerche, Cagliari, Italy

## ABSTRACT

Seven male competitive road cyclists ( $22.3 \pm 3.2$  years;  $73.9 \pm 5.5$  kg;  $185 \pm 7.9$  cm), with  $7.0 \pm 6.8$  years of racing experience and approximately 7 hours per week of specific training, participated in a laboratory-based cardiopulmonary incremental test to exhaustion. Each cyclist performed the test on their personal bicycle, with the rear wheel replaced by an electromechanical system that allowed real-time measurement of the mechanical power output generated during pedaling. Throughout the test, beat-by-beat cardiovascular variables—including stroke volume, heart rate, and cardiac output—were continuously assessed noninvasively using a custom-designed wearable device based on electrical impedance cardiography. Using proprietary telemedicine software, bioimpedance data collected during the tests were transmitted for remote acquisition and processing by an expert medical team. The experimental sessions were conducted in a dedicated laboratory of the Department of Mechanical and Aerospace Engineering at the Polytechnic University of Turin, Italy. The results demonstrated a progressive increase in cardiac output up to exhaustion, driven by concurrent increases in heart rate and stroke volume. The rise in stroke volume was attributed to enhanced myocardial contractility and the maintenance of ventricular preload. Mean arterial blood pressure remained stable until the end of the test, despite a substantial decrease in diastolic pressure.

Keywords: road cyclists, cardiopulmonary test, impedance cardiography, cardiac output

## 1 INTRODUCTION

In cycling sports, one of the main objectives is to accurately measure the power output developed on the bicycle during training or competition. In the 1980s, Ulrich Schoberer

developed the “SRM spider” device [1], which, when mounted on a bicycle, allows the mechanical power produced during cycling performance to be measured with very high precision [2]. These technological innovations made it possible to investigate how the various physiological systems involved in cycling performance interact, by enabling the formulation of rigorous mathematical correlations between the stimulus variable—namely, the mechanical power applied to the pedals—and circulatory, respiratory, and metabolic responses. Advances in modern wearable technologies now make it possible not only to improve the quality of life of individuals affected by severe disabling pathologies [3–7], but also to enable real-time, quantitative assessment of the respiratory and metabolic

---

Contact authors: Filippo Tocco<sup>1</sup>, Alberto Concu<sup>2</sup>

<sup>1</sup>Dept of Medical Sciences and Public Health, University Cittadella, Provincial Road 8 – 09042 Monserrato (CA), Italy;

<sup>2</sup>AC Technologies Ltd, Via Pais 12- 09128 Cagliari, Italy.

adjustments [8–10] of athletes during laboratory simulations of different racing conditions. However, precise measurement of cardiodynamic variables during motion has remained challenging, as current techniques still lack sufficient accuracy under dynamic conditions. Nevertheless, a non-invasive method has been available for some time: electrical impedance cardiometry (EIC) [11, 12]. This technique enables the beat-to-beat assessment of cardiac output along with the cardiodynamic variables on which it depends, even in moving subjects through the use of wearable devices [13–16]. In the present study, competitive road cyclists employed the EIC method to monitor progressive changes in their cardiodynamic profile. Specifically, they wore a custom-made EIC wearable device, the E-Physio Tool [16–18], while performing a cardiopulmonary incremental exercise test to exhaustion in a laboratory setting. The test was conducted using each cyclist’s own bicycle, with the rear wheel replaced by an ergometer capable of precisely measuring the mechanical power applied to the pedals. Some of the data presented here have been previously reported in a master’s thesis in Mechanical Engineering at the *Politecnico di Torino*, Italy [19].



Figure 1 Promotional image from an advertising flyer illustrating the use of the Elite Direto XR-T power meter. The device replaces the rear wheel of the athlete’s bicycle and connects directly to the cassette, which interacts with the derailleur and chain to enable gear shifting and maintain optimal pedalling efficiency across various terrains.

## 2 METHODS

### 2.1 SUBJECTS

Seven road racing competitive skilled cyclists were engaged and their characteristics are shown in table I.

Table I – Morphological and training data

Age (years)	BM (kg)	BH (cm)	Cycle <sub>Pract</sub> (years)	Time <sub>weeclly</sub> (h:min)
22.3	73.9	185	7.0	6:45
±3.2	±5.5	±7.9	±6.8	±0:21

BM: body mass; BH: body height; Cycle<sub>Pract</sub>: practice of cycling; Time<sub>weeclly</sub>: time at week spent in cycling training in hours and minutes. Each athlete was made aware about the experimental procedure and all of them declared their informed consent.

### 2.2 INSTRUMENTATION

#### 2.2.1 Mechanical equipment.

The Elite Direto XR-T power meter (Elite Ltd., Italy) was selected for this study. This device replaces the bicycle’s rear wheel, allowing the bike to connect directly to its cassette (Figure 1). A constant resistance torque mode was employed, and the cyclists self-regulated their cadence and gear ratios during the trials. Each athlete used their own bicycle to prevent improper pedaling mechanics that could result from an incorrectly sized frame [20]. This mechatronic system communicates with smartphones via ANT+ technology (ANT-Productions, Belgium), a wireless communication standard commonly used for data transmission between fitness devices. Through this connection, the system recorded the cyclist’s speed, pedaling cadence, and power output. The acquired data were stored on a Garmin cycle computer (Garmin, Lenexa, KS, USA) and subsequently

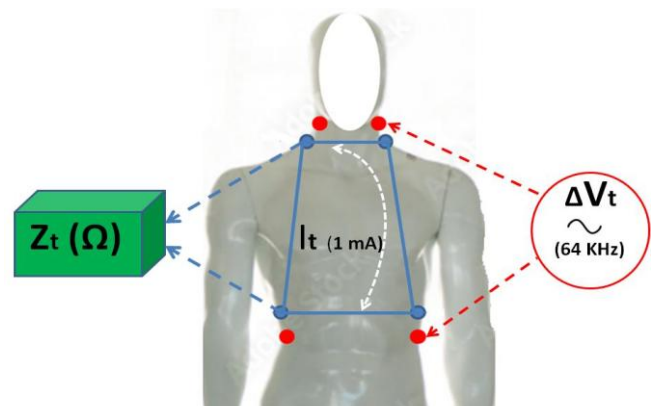


Figure 2 Schematic representation, on a mannequin, of the application of the E-Physio Tool to the human thorax. The device models an inverted truncated cone whose smaller circumference lies in the plane of the roots of the neck muscles, while the larger circumference lies in the plane of the xiphoid process. The blue trapezium represents the core of the volume of electrically participating tissues (VEPT) contributing to the thoracic impedance. Two pairs of disposable electrodes (blue circles), positioned respectively at the smaller and larger circumferences, enable the acquisition of beat-to-beat thoracic electrical impedance values ( $Z_t$ ) using the impedance measurement device (indicated by blue dotted arrows). This measurement is made possible by the E-Physio Tool, which applies an electrical potential difference ( $\Delta V_t$ ) through two additional pairs of disposable electrodes (red circles and red dotted arrows), placed a few centimetres outside the measurement electrodes. This configuration generates within the thorax an alternating electrical current ( $I_t$ ) of constant amplitude (1 mA at 64 kHz), symbolised by the white dotted line within the trapezium.



Figure 3 Analog traces of bioimpedance variables recorded by the LabCart Reader from a cyclist at rest. From top to bottom, the plots show: (1) beat-to-beat thoracic bioimpedance signals, in which the main, broader, and slower harmonic corresponds to the respiratory rate (see the two blue arrows marking the beginning and end of a breath), while the superimposed, narrower harmonic—synchronous with the cardiac cycle—represents the beat-to-beat variations in thoracic bioimpedance, which are clearly isolated in the second trace; (2) the first mathematical derivative of thoracic bioimpedance in the third trace; and (3) the beat-to-beat electrocardiogram in the fourth trace.

analyzed using the *Strava software* (Strava Inc., San Francisco, CA, USA). Strava is a widely used fitness-tracking and social networking application for athletes that records workouts such as running, cycling, and swimming using GPS data. The use of this mechatronic equipment is supported by previous validation studies [21, 22]. In this study, the software integrated into the mechatronic device enabled the assessment of mechanical power output during cycling performance at each pedaling phase.

### 2.2.3 Biomedical equipment.

The E-Physio Tool is a device that, as shown in Figure 2, applies a low-intensity, high-frequency alternating electrical current ( $I = 1 \text{ mA}$ ,  $64 \text{ kHz}$ ), powered independently by a power bank supplying up to  $2 \text{ mA}$  at  $5 \text{ V}$ , along the planes corresponding to the roots of the neck muscles and the xiphoid process. The resulting difference in electric potential between these two points ( $\Delta V_t$ ) is then measured.

The reliability of data acquired using this EIC device was demonstrated in a previous study [23], where it was compared with a validated EIC (NCCOM3-R7, BoMed, CA, USA) previously cited in the scientific literature (see references 15 and 16 in [23]). Stroke volume (SV) values were obtained by both instruments in 18 male participants at rest and during exercise up to 70% of their age-predicted maximum heart rate ( $220 - \text{age}$ ).

Agreement between the two measurement methods was assessed using the Bland–Altman analysis from the ICT wearable device and the NCCOM3, both at rest and during exercise. The limits of agreement were within  $+7.01$  and  $-8.12 \text{ mL}$  at rest, and  $+6.77$  and  $-9.86 \text{ mL}$  during exercise.

Thus, this approach allowed the calculation of the real component of thoracic impedance ( $Z_t$ ) using the following equation, as the imaginary capacitive reactance was effectively nullified by the very high frequency of the alternating electrical current.

$$Z_t = \Delta V_t / I_t \quad (1)$$

Thanks to the open-source LabChart Reader, both the  $Z_t$  and ECG signals could be acquired non-invasively on a beat-to-beat basis using electrodes placed on the athletes' thorax and visualized in real time on a PC screen. As shown in Figure 3, the LabChart software enabled the acquisition of the following conditioning variables related to left ventricular SV: TFI ( $Z_t^{-1}$ , or thoracic fluid index), representing the electrical equivalent of left ventricular preload (LVPL); EVI (electrical equivalent of left ventricular ejection velocity peak), here considered as the myocardial contractility index (MCI); and ventricular ejection time (VET). The Sramek-Bernstein equations (2 and 3) allow indirect calculation of SV as follows [24, 25]:

$$SV = TFI \times EVI \times VET \times VEPT \quad (2)$$

$$SV = (\Omega^{-1}) \times (\Omega \text{ s}^{-1}) \times (s) \times (\text{cm}^3) = \text{cm}^3 \quad (3)$$

Equation (2), in addition to three multipliers of purely bioimpedance origin, includes a fourth multiplier: the volume of electrically participating tissues in the thoracic impedance (VEPT). VEPT was derived from a nomogram based on the subject's anthropometric characteristics weight,

height and sex, as described by Donald Bernstein experimental tests [24]. Equation (3) further demonstrates that, from a dimensional perspective, the product of these four variables on the right-hand side of the equation yields a volume (cm<sup>3</sup>), corresponding to the volume of blood ejected by the left ventricle into the aorta during each systole.



Figure 4 Image of a tested cyclist, assisted by two skilled operators from the Polytechnic University of Turin, Italy, while pedaling on his bike. (1) The rear wheel has been replaced with an Elite Direto XR-T power meter (not visible in the image). (2) Tablet organizer held by one of the operators for acquiring mechanical and biomedical measurements, the latter manually recorded by both operators. (3) Finger pulse oximeter. (4) Disposable ECG electrode visible here, attached at the roots of the neck muscles. (5) Inflatable sphygmomanometer cuff with stethoscope, used by the other operator to auscultate brachial artery sounds. (6) Box containing the E-Physio impedance cardiograph hardware and electronics. (7) Five-pin connection cable linking the athlete's chest electrodes to the impedance cardiograph. (8) Power bank providing 5 V, 2.4 A DC supply to the impedance cardiograph. (9) Garmin Edge cycle computer.

As is known, multiplying SV to the heart rate per minute (HR), it can be calculated the CO as:

$$CO = SV (ml) \times HR (beats \min^{-1}) = mL \min^{-1} \quad (4)$$

### 2.3 EXPERIMENTAL PROTOCOL

Each recruited cyclist performed an incremental test, pedaling their bicycle connected at the rear to the Elite Direto XR-T cycle-ergometer power meter (see Figures 1 and 4)

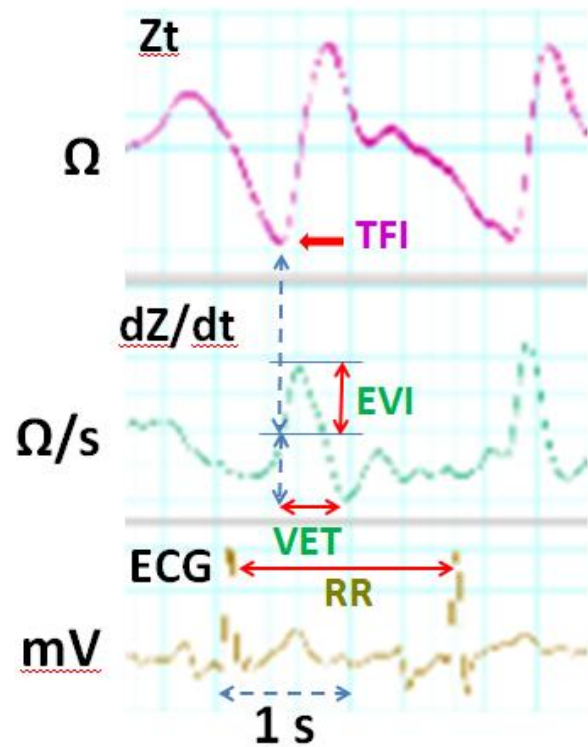


Figure 5 The graphs in the figure are enlarged segments of the impedance recordings obtained with the LabCart Reader during a cardiac cycle in one of the tested cyclists. The top panel shows the thoracic impedance ( $Z_t$ ) variations, where the minimum value (indicated by a red arrow) represents the thoracic fluid volume index (TFI). The reciprocal of this value corresponds directly to the left ventricular end-diastolic volume (ventricular preload). The subsequent diastolic wave corresponds to the closure of the aortic valve at the end of ventricular ejection. The middle panel displays the first derivative of  $Z_t$  ( $dZ/dt$ ), where the peak corresponds to the maximum impedance index of the EVI, and the VET indicates the left ventricular ejection time. The bottom panel shows the ECG trace, with the R-R interval corresponding to the duration of the cardiac cycle analyzed.

until they were unable to continue. Cyclists self-selected their pedaling cadence, while the pedal load, starting at 0 W, increased by 30 W every 2 minutes. At each stage of the test, systolic and diastolic blood pressures were measured using a manual sphygmo-manometer (PB Pharma, Metal Deluxe, Italy) via the auscultatory Riva-Rocci-Korotkoff method [26] with a stethoscope (Figure 6). Arterial oxygen saturation ( $SO_2$ ) was simultaneously recorded using a commercial fingertip device. For each athlete, the workload measured during the last minute of each stage was considered the maximal workload ( $W_{max}$ ). Data collected remotely through the E-Physio Tool required careful review and selection to obtain accurate values for the variables of interest. Impedance cardiography recordings were provided in “.txt” format, and to visualize them as time-analogous traces, the “LabChart Reader” program was used [27]. Once opened, the software allowed visualization (Figure 3) of the beat-to-beat evolution of two primary variables:  $Z_t$  and ECG.



Figure 6 On the left, the manual sphygmomanometer is shown, comprising three main components: an inflatable arm cuff, a rubber bulb with a valve for air inflation and deflation, and an aneroid manometer for displaying pressure readings. On the right, the stethoscope is depicted, consisting of a small, disc-shaped chest piece (diaphragm or bell) placed over the brachial artery beneath the cuff to capture sounds, which are then transmitted through flexible tubing to the earpieces worn by the user.

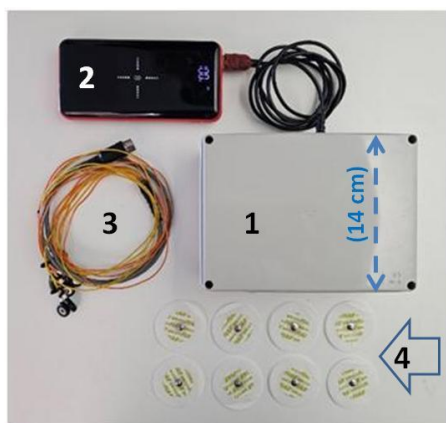


Figure 7 The custom designed “E-Physio Tool” is shown, with the main device unit (1) connected by a cable to its power bank (2). The patient connection cable (3) is shown coiled; it connects to the device via a 5-pin plug and terminates in 8 snap connectors on the opposite end, which attach to the eight disposable electrodes (4) placed on the patient’s chest.

Using LabChart, the first derivative of  $Z_t$  ( $dZ_t/dt$ ) was also analyzed. With a specific graphical cursor (Figure 5), both the EVI and VET were calculated beat-to-beat from the  $dZ_t/dt$  trace. Together with the reciprocal of  $Z_t$ , these represent the three impedance-based components of the Sramek-Bernstein equation. From the ECG trace, heart rate (HR) per minute was calculated based on the R-R interval, and breath-by-breath respiratory rate (BR) was also determined (Figure 3). For each measurement interval corresponding to a test stage, variables of interest were averaged over 10 consecutive beats, starting from the first beat after the midpoint of the stage, to minimize the influence of inaccurate measurements. Special care was taken to eliminate outliers, which are common at high workloads. For each stage, from  $W_0$  to  $W_{max}$ , 20 consecutive measurements were initially recorded. Outliers and values most deviant from the mean were removed, and the remaining 10 measurements were averaged. This procedure also substantially reduced the standard deviation of stage-specific variables.

## 2.4 REMOTE DATA ASSESSMENT

A key feature of the E-Physio tool (Figure 7) is that it functions as an Internet of Things (IoT) device with the capability to connect to the internet. This connectivity enables real-time data transmission and reception, facilitating interaction and communication with other remote devices and systems. Another important aspect of the E-Physio tool is its ability to be managed and controlled remotely via web-based platforms. Thus, the E-Physio tool is an IoT system equipped with sensors and actuators that allow it to both collect data from the physical environment and interact with it. Specifically, it can detect multiple cardiorespiratory variables in subjects tested remotely, providing detailed information on their cardiovascular and respiratory profiles. In these experiments, skilled physicians and researchers operating in the biomedical laboratory of AC Technologies Ltd. (ACTlab, Italy) remotely acquired cardiodynamic data transmitted from the biomechanics laboratory at the Department of Mechanical and Aerospace Engineering, Polytechnic University of Turin (DIMlab, Italy), via the E-Physio tool and other connected devices. The data were obtained from a cyclist undergoing an incremental test, continuously monitored by two expert technicians (see Figure 4). During both the athletes’ pre-test preparation and the test execution, a continuous real-time audio-visual communication was maintained between the two remote research units, located in the ACTlab and the DIMlab, to ensure proper adherence to the experimental protocol.

## 3 RESULTS

To better illustrate the functional adjustments observed in the cyclists during the test, the step-by-step changes of each selected variable are graphically represented below, using one of the subjects as a reference. In these graphs, the standard deviations (previously shown to be negligible) were omitted for each workload increment, in order to make the characteristic curves clearer and easier to interpret, thereby emphasizing their descriptive value. Figure 8 shows that the breathing rate (BR) initially increased almost linearly with the progressive workload, starting from approximately 13 breaths/min at 90 W ( $W_0$ , 6<sup>th</sup> minute) up to the 24<sup>th</sup> minute (1<sup>th</sup> step), which was of 330 W. Beyond this point, the slope of the increase became steeper, reaching the maximum BR at  $W_{max}$  (390 W) after only two additional workload increments. The figure also indicates that after about 10 minutes of recovery, the BR nearly returned to its resting value (13.5 vs. 17.8 breaths/min, respectively). In Figure 9, HR increased sharply from 62 b/min at  $W_0$  to 110 b/min at the fourth workload step, corresponding to the 10<sup>th</sup> minute from the beginning of the test. After this point, HR continued to rise at a nearly steady rate, reaching 163 b/min at  $W_{max}$ , although with a gentler slope of approximately 3 b/min per step. In contrast to the behavior observed for breathing rate (BR), after the de-fatiguing pedaling period HR did not return to its pre-test value, remaining instead at 102 b/min. Figure 10 illustrates the workload-induced behavior of the

athlete's systolic (SABP) and diastolic (DABP) arterial blood pressures. The SABP increased in a pattern similar to that observed for heart rate (HR), rising from 122 Torr at  $W_0$  to a peak of 185 Torr at  $W_{max}$ . In contrast, the DABP exhibited an opposite trend, decreasing progressively from 80 Torr at  $W_0$  to a minimum of 15 Torr at  $W_{max}$ . During the recovery pedalling period, the SABP nearly returned to its resting value (118 Torr), whereas the DABP did not fully recover, stabilizing instead at 60 Torr. The blue curves in Figures 11, 12, and 13 illustrate the workload-dependent changes in three bioimpedance-derived variables contributing to the SV generation: the Thoracic Fluid Index or TFI, the Ejection Velocity Index or EVI, and the Ventricular Ejection Time or VET, respectively.

In Figure 11, the TFI curve shows an initial increase in the LVPL, rising from its resting value of  $41.8 \text{ m}\Omega^{-1}$  up to  $43.8 \text{ m}\Omega^{-1}$  at the fourth workload step—an increase of approximately +5%. Beyond this point, TFI remained stable until the peak workload was reached. However, during the post-exercise (de-fatiguing) pedalling period, TFI decreased to  $40.8 \text{ m}\Omega^{-1}$ , corresponding to about -2.8% relative to its resting value. In contrast, the blue curve in Figure 12, which represents the workload-induced changes in the cyclist's EVI (here considered as the left ventricular MCI), displays an increasing trend similar to that observed in the BR. From rest ( $W_0$ ,  $1.21 \text{ }\Omega \cdot \text{s}^{-1}$ ) up to the 22<sup>nd</sup> minute of pedalling ( $2.49 \text{ }\Omega \cdot \text{s}^{-1}$ ), EVI increased almost linearly, at a rate of approximately  $0.13 \text{ }\Omega \cdot \text{s}^{-1}$  per step. After this point, the slope steepened, leading to a peak value of  $3.07 \text{ }\Omega \cdot \text{s}^{-1}$ . As shown by the blue curve in Figure 13, the cyclist's VET during the incremental test behaved, as expected, inversely to HR. Specifically, compared to the resting value (0.182 s), VET decreased markedly during exercise, reaching 0.138 s at maximal workload ( $W_{max}$ )—a reduction of approximately 24%. The blue curve in Figure 14, representing the stroke volume (SV) adjustments observed in this athlete during the test effort—resulting from the integrated responses of TFI, EVI, and VET—displays a triphasic pattern.

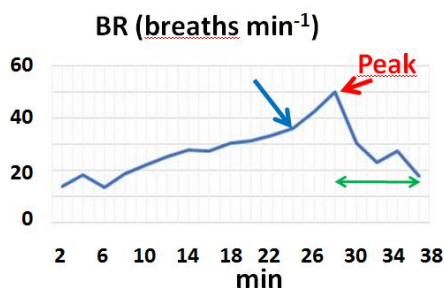


Figure 8 In the representative subject selected as a reference, the blue curve illustrates the breathing rate (BR), measured every 2 minutes from the beginning of the incremental test until exhaustion. The interval between the two tips of the double green arrow indicates the de-fatiguing pedalling period. The blue arrow marks the time point from the beginning of the test when the curve slope sharply increased (approximately at the 23<sup>rd</sup> minute), up to the workload peak indicated by the red arrow.

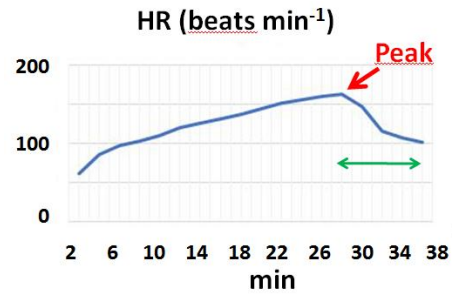


Figure 9 In the tested subject, the blue curve shows the heart rate (HR), measured every 2 minutes from the start of the incremental test until exhaustion. The interval between the two tips of the double green arrow indicates the de-fatiguing pedalling period. The red arrow marks the time point at which the peak mechanical power output occurred. From the 6<sup>th</sup> minute up to the peak workload, no significant changes in the curve slope were observed.

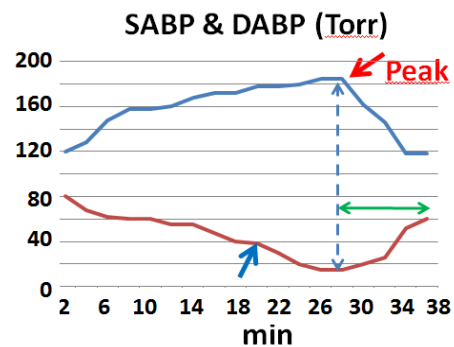


Figure 10 In the same subject, the blue and red curves represent the systolic (SABP) and diastolic (DABP) arterial blood pressures, respectively, measured every 2 minutes from the beginning of the incremental test until exhaustion. The blue vertical dotted line indicates the coincidence of both pressures at the peak workload step, marked by the red arrow. The blue arrow highlights the point (around the 20<sup>th</sup> minute) at which the DABP curve showed an increase in its negative slope. The interval between the two tips of the double green arrow represents the de-fatiguing pedalling period for both arterial pressure variables.

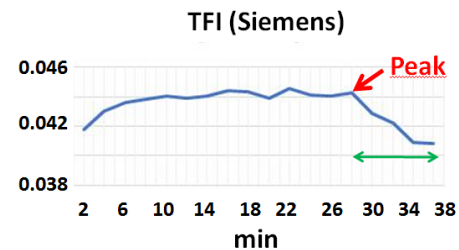


Figure 11 In the tested subject, the blue curve represents the thoracic fluids index (TFI)—that is, the left ventricular preload index—measured in Siemens as thoracic electrical conductance, assessed every 2 minutes from rest up to the peak workload during the incremental test to exhaustion. The interval between the two tips of the double green arrow indicates the de-fatiguing pedalling period. The red arrow marks the time at which the peak mechanical power output occurred.

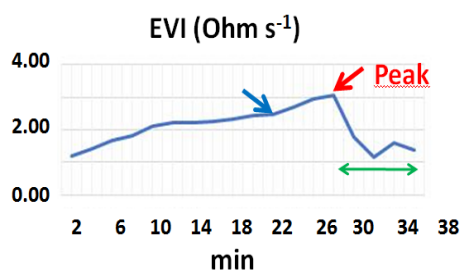


Figure 12 In the representative cyclist, the blue curve illustrates the left ventricular ejection velocity index (EVI), assessed every 2 minutes from the beginning of the incremental test until exhaustion. The interval between the two tips of the double green arrow indicates the de-fatiguing pedalling period. The blue arrow marks the time point when the curve slope visibly increased (approximately at the 22<sup>th</sup> minute), while the red arrow indicates the time corresponding to the peak mechanical workload.

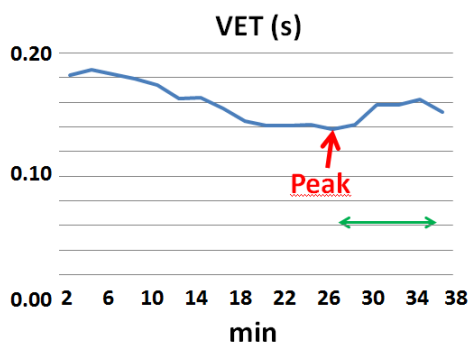


Figure 13 In the here tested cyclist, the blue curve shows the left ventricular ejection time (VET), measured every 2 minutes from the beginning of the incremental test until exhaustion, indicated by the red arrow. The interval between the two tips of the double green arrow indicates the de-fatiguing pedalling period.

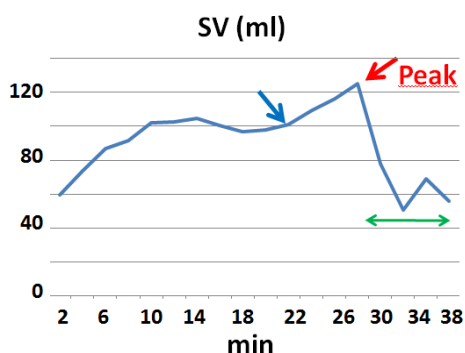


Figure 14 In this cyclist, the blue curve represents the left ventricular stroke volume (SV), measured every 2 minutes from the beginning of the incremental test until exhaustion. The interval between the two tips of the double green arrow indicates the de-fatiguing pedalling period. The blue arrow marks the point where an increase in the curve slope occurred, while the red arrow indicates the time at which the peak mechanical power output was reached.

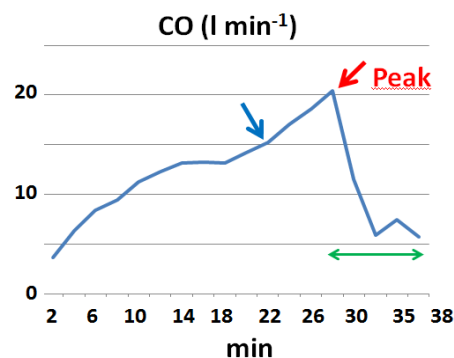


Figure 15 In the representative cyclist, the blue curve illustrates the cardiac output (CO), measured every 2 minutes from the beginning of the incremental test until exhaustion. The interval between the two tips of the double green arrow indicates the de-fatiguing pedalling period. The blue arrow marks a small but evident increase in the curve slope, while the red arrow indicates the time corresponding to the peak mechanical power output.

From rest to the 10<sup>th</sup> minute of exercise (corresponding to the 5<sup>th</sup> workload step), SV increased from 59.7 ml to 102.5 ml, 100 ml, fluctuating between a minimum of 96.6 ml and a maximum of 104.5 ml. Subsequently, as indicated by the blue arrow in figure, at approximately the 22<sup>th</sup> minute, SV rose sharply again, with a mean slope of about 8.5 mL per step during the final three workload increments, ultimately reaching a peak value of 125.2 ml. However, by the end of the recovery (de-fatiguing) phase, SV returned to its resting value, even dropping slightly below it. As is well known, CO depends on both an inotropic component (SV) and a chronotropic component (HR), being mathematically defined as their product (see Eq. 4). Indeed, as shown in Figure 15, the morphology of the cyclist's CO curve as a function of workload increase resembles the shape of the SV curve, albeit with less pronounced variations in slope, due to the smoothing effect of HR. Nevertheless, as highlighted by the blue arrow in Figure 15, a small but noticeable increase in the CO curve slope also occurred when the workload reached the 22<sup>th</sup> minute from  $W_0$ . At the end of the post-test recovery period, however, CO did not return to its resting value, remaining at  $5.7 \text{ l min}^{-1}$  compared to the resting level of  $3.7 \text{ l min}^{-1}$ . Table II reports the mean  $\pm$  SD values of all selected cardiorespiratory variables measured in the seven cyclists, both at  $W_0$  and at  $W_{\max}$ . A statistically significant increase was observed at  $W_{\max}$  compared with  $W_0$  for HR, BR, SABP, EVI, SV, and CO, whereas DABP, and VET significantly decreased. In contrast, no statistically significant change was found in TFI between  $W_{\max}$  and  $W_0$ . Furthermore, a slight reduction in peak  $\text{SO}_2$  was observed ( $-2\%$ ), although this variation remained within the range of physiological variability. Nevertheless, due to the small sample size of the tested subjects, the only statistically significant differences observed between mean resting and peak values (i.e.,  $W_0$  and  $W_{\max}$ ;  $P < 0.5$  or  $P > 0.5$ ) may not fully capture the true effect size produced by the incremental test performed to exhaustion.

Table II – Mean  $\pm$  SD values of cardiorespiratory variables among seven tested athletes

STEP	W (watt)	HR (Beat/min)	BR (Breath/min)	SABP (Torr)	DABP (Torr)	SO <sub>2</sub> (%)	TFI (Siemens)	EVI ( $\Omega$ /s)	VET (s)	SV (ml)	CO (l/min)
W <sub>0</sub>	0	67	17	122	74	98	0.044	1.12	0.22	74.3	4.6
$\pm$ SD		$\pm$ 11	$\pm$ 2	$\pm$ 10	$\pm$ 8	$\pm$ 1.0	$\pm$ 0.002	$\pm$ 0.11	$\pm$ 0.03	$\pm$ 1.1	$\pm$ 0.2
W <sub>max</sub>	360	182*	56*	194*	38*	96*	0.043	3.27*	0.14*	131.4*	21.3*
$\pm$ SD	$\pm$ 36	$\pm$ 11	$\pm$ 8	$\pm$ 12	$\pm$ 19	$\pm$ 1.4	$\pm$ 0.004	$\pm$ 0.29	$\pm$ 0.01	$\pm$ 26.5	$\pm$ 5.5
$\Delta$ %		+172	+229	+59	-49	-2	-2.3	+192	-36	+77	+363

W<sub>0</sub>: rest; W<sub>max</sub>: maximum workload; HR: heart rate; BR: breath rate; SABP: systolic arterial blood pressure; DABP: diastolic arterial blood pressure; SO<sub>2</sub>: arterial blood oxygen saturation; TFI: thoracic fluids index; EVI: ejection velocity index; VET: ventricular ejection time; SV: stroke volume; CO: cardiac output;  $\Delta$ %: changes in percentage of maximum versus rest values; \*: P<0.05 or statically significant compared to rest (the Student's *t* parametric test for paired data was here utilized).

Table III – Effect sizes amplitude of the W<sub>max</sub> versus W<sub>0</sub> mean values comparisons for each selected variable

Variables	Means difference (W <sub>max</sub> -W <sub>0</sub> )	Pooled SD	Cohen's "d" index
HR Beats/min	115	11.00	10.45
BR Breaths/min	39	5.83	6.69
SABP Torr	72	11.04	6.52
DABP Torr	-36	14.58	12.11
SO <sub>2</sub> %	2	1.22	1.64
TFI mSiemens	1	3.46	0.29
EVI m $\Omega$ /s	2150	219	9.82
VET ms	-80	22.36	3.58
SV ml	57.10	18.75	3.04
CO l/min	16.7	3.90	3.89
Workload W	360	25.46	14.14

HR: heart rate; BR: breath rate; SABP: systolic arterial blood pressure; DABP: diastolic arterial blood pressure; SO<sub>2</sub>: arterial blood oxygen percentage; TFI: thoracic fluids index; EVI: peak of left ventricle ejection velocity index; VET: ventricular ejection time; SV: left ventricle stroke volume; CO: cardiac output.

Therefore, the Cohen's "d" index [28]—calculated as the difference between the two means divided by the pooled standard deviation—was employed. For each cardiorespiratory and power-related variable considered, table III reports the magnitude of this effect when comparing values at W<sub>0</sub> and W<sub>max</sub>. A "d" value greater than 0.8 was interpreted as indicating a strong physiological response of the variable to maximal exercise, which was the case for all but one of the variables analyzed.

Conversely, a "d" value around 0.2, as observed for TFI, suggests a negligible effect size between W<sub>max</sub> and W<sub>0</sub>, implying that these two conditions are practically similar for this variable.

#### 4 DISCUSSION

Data presented in Table II clearly demonstrate that the group of competitive road cyclists investigated in this study were characterized by cardiodynamic profiles typical of well-trained athletes engaged in this sport. Recent evidence indicates that the functional adaptations occurring during exercise in such athletes are characterized by increased hemodynamic force generation during systole and enhanced relaxation during early diastole [29]. Indeed, the cardiovascular variables that primarily determined the cyclists' oxygen consumption—and consequently their muscular power output—namely the cardiac output "CO", which was in turn dependent on the SV and, more specifically, on the EVI, all reached peak values significantly higher than those observed at rest. These differences were statistically significant both in terms of "P" and "d" values here calculated. Furthermore, in the representative athlete's graphs showing the changes in these three cardiodynamic variables with increasing workload, a marked increase in the slope of the curves becomes evident at approximately 77% (300 W) of the maximal workload (W<sub>max</sub> = 390 W). Simultaneously, the curve describing the BR as a function of workload also shows a noticeable increase in slope beginning around 330 W compared with the W<sub>0</sub> condition. Considering that during exercise pulmonary ventilation (PV) is mainly driven by BR [30], and that during incremental exercise PV increases its slope when carbon dioxide volume (VCO<sub>2</sub>) production exceeds that of oxygen uptake (VO<sub>2</sub>)—that is, when the so-called aerobic threshold (AT) is reached [31]—the observed increase in the slope of the BR curve in the studied athlete can reasonably be interpreted as an indicator of having reached the AT. Sendra-Perez et al. [32], studying skilled cyclists and triathletes performing an incremental test on a cycle ergometer, reported that muscle oxygen saturation—corresponding to the attainment of the AT—in the biceps femoris occurred at approximately 77% of W<sub>max</sub>. This percentage closely matched the workload at which an increased slope was observed in the cardiodynamic

variables of our tested cyclist. Accordingly, the cyclist's CO and its generating cardiodynamic components—namely, EVI and SV—all exhibited slope increases in their respective characteristic curves around the workload corresponding to a metabolic substrate shift. This shift reflects the point at which anaerobic pathways begin to play a crucial role in supplying energy for the mechanical power produced by the pedalling muscles. From this observation, it can be inferred that this experimental protocol allows for the detection of the percentage of  $W_{max}$  at which AT occurs in competitive road cyclists directly from the morphology of the cardiodynamic response curves during an incremental test. Thus, it eliminates the need for bulky and expensive calorimetric equipment for measuring  $O_2$  consumption and  $CO_2$  production in performing athletes. In this context, it is well known that just above the AT, enhanced sympathetic activity promotes the secretion of hormones (e.g., epinephrine) that increase heart rate and blood pressure to sustain oxygen delivery to the tissues. Moreover, a recent study demonstrated a strong relationship between the rapid repolarisation of the cardiac ventricles—triggered by the heightened sympathetic drive—and the attainment of AT. Specifically, upon reaching AT during an incremental test, the surge in sympathetic activity required for faster ventilation induces rapid changes in sympathetically modulated ventricular repolarisation [33]. It is therefore reasonable to hypothesize that, in our exemplified cyclist, the rapid electrical event of ventricular repolarisation was followed by an equally rapid mechanical response of the ventricle—manifested as an increase in myocardial contractility, which translates into a higher velocity of left ventricular ejection. In our study, the blue arrows in the EVI, followed by SV and then CO characteristic curves plotted against increasing workload, indicate a steeper slope after the subject's AT, or approximately at 80% of  $W_{max}$ . When extrapolated from individual athletes to the average of all seven tested subjects, these data confirm that all participants had excellent aerobic capacity, efficiently supplying energy to the muscles involved in sustaining high pedal workloads. This performance was further supported by a cardiodynamic contribution, as CO increased post-AT, thereby enhancing oxygen delivery to the working muscles. However, considering the heterometric contribution of ventricular preload (see the TFI graph in Figure 11) to SV and consequently to CO, it is evident that TFI initially increased by approximately 5% above the resting value with workload rising to 120 W and then remained essentially unchanged up to  $W_{max}$ . In summary, the two central/cardiac determinants of SV—the homeometric component, reflecting sympathetic nervous system-mediated myocardial contractility as represented by EVI, and the heterometric component, reflecting mechanical volumetric properties as represented by end-diastolic ventricular volume index by TFI—both increased during exercise on the laboratory bicycle. This dual contribution explains the progressive increase in SV despite a gradual reduction in VET, which decreased from 0.18 s at  $W_0$  to approximately 22% below the resting value around 70% of  $W_{max}$ , and remained stable

thereafter until peak workload (see Figure 13). The resultant SV, together with the nearly linear increase in HR, substantially contributed to the observed progressive rise in CO. During acute aerobic exercise, left ventricular diastolic function, and consequently ventricular filling, increase to ensure adequate cardiac output. This represents a significant challenge for the myocardium because exercise-induced tachycardia shortens ventricular diastolic time, even as cardiac output must rise to meet physiological demands [34]. In contrast to acute exercise, chronic exercise training, as observed in the exemplified cyclist in our study, has been shown to enhance myocardial diastolic function [35]. As diastolic time shortens with increasing exercise intensity, the diastolic filling rate must rise to maintain the balance between left ventricular filling and ejection. This increase in diastolic filling rate is achieved primarily by augmenting the trans-mitral diastolic pressure gradient between the left atrium and left ventricle. The trans-mitral flow rate rises due to a relative decrease in intra-left ventricular pressure during early diastole [35], effectively creating a left ventricular suction effect across the mitral valve that enhances the trans-mitral pressure gradient. Several mechanisms contribute to this left ventricular diastolic suction:

1. Increased systolic contractile force (inotropic effect) enhances early diastolic elastic recoil of the myocardium [36].
  2. Greater systolic fiber shortening during exercise results in smaller end-systolic volumes and lower intra-left ventricular pressures during early diastolic filling [37].
  3. Enhanced relaxation of individual cardiomyocytes which occurs due to increased sarcoplasmic reticulum (SR) calcium reuptake [38], which is further stimulated by exercise-induced beta-adrenergic activation [39].
  4. Beta-adrenergic stimulation increases cyclic AMP, which phosphorylates phospholamban, a regulatory of the SR membrane protein. This phosphorylation accelerates SR calcium reuptake, thereby enhancing cardiomyocyte relaxation and increasing the rate of diastolic filling [39,40].
- Since the normal heart can increase trans-mitral diastolic flow during exercise through enhanced ventricular contraction and relaxation (ventricular suction), it can be reasonably inferred that, in the present sample of cyclists, the maintenance—or even increase—of left ventricular preload during the test, despite the progressive shortening of diastolic time, reflects a coordinated set of morpho-functional adaptations.

These adaptations are characteristic of athletes extensively trained for long-duration aerobic activities such as road cycling. Moreover, in this type of cyclist, the potential contribution of reduced total peripheral vascular resistance (TPVR)—i.e., left ventricular afterload—to the increase in SV during intense exercise should not be overlooked. TPVR at a given workload can be estimated as the ratio between mean arterial blood pressure (MABP) and CO. MABP can, in turn, be calculated as [41]:

$$MABP = DABP + 1/3 (SABP - DABP) = Torr \quad (5)$$

thus the TPVR could be obtained as [41]:

$$TPVR = MABP : CO = \text{Torr min l}^{-1} \quad (6)$$

Concerning our reference cyclist, data from Figure 10 indicate that the MABP at  $W_0$  was 90 Torr, and data from Figure 15 show that the corresponding CO was  $3.7 \text{ l min}^{-1}$ . Consequently, the TPVR at  $W_0$  was approximately  $24.3 \text{ Torr min l}^{-1}$ . At  $W_{\max}$ , his MABP remained at 90 Torr, while the corresponding CO increased to about  $20 \text{ l min}^{-1}$ , resulting in a TPVR of  $4.5 \text{ Torr min l}^{-1}$ —roughly 18% of its value at  $W_0$ .

This marked reduction in TPVR with increasing workload may appear paradoxical, given that exercise generally induces a widespread increase in sympathetic tone, leading to  $\alpha_1$ -adrenergic receptor-mediated vasoconstriction across most vascular beds. However, it has been shown [42] that  $\alpha_1$  receptors are predominantly located in large upstream arteries of the muscles and are less sensitive, or even insensitive, to inhibitory factors generated by muscle metabolism. This distribution contributes to the maintenance of high MABP values as exercise intensity increases, as described by the following equation:

$$MABP = TPVR \times CO \quad (7)$$

Thus, maintaining—or at least not allowing a decrease in—MABP during incremental exercise (as was observed in our tested cyclist) helps ensure adequate arterial blood flow to the working muscles by sustaining sufficient CO values, as illustrated by the following equation:

$$CO = MABP : TPVR \quad (8)$$

At the same time, due to the high density of  $\alpha_2$ -type adrenergic receptors in intramuscular arteries—which serve a nutritive function and are highly sensitive to inhibition by muscle-derived agents/catabolites such as prostaglandins, adenosine, thromboxanes, and others—there is consequent intramuscular vasodilation aimed at supplying nutrients to the myocytes [43]. In the reference cyclist analyzed here, the graphs in Figure 10 clearly show two opposing events as workload increased: (a) a progressive rise in SABP resulting from increasing  $\alpha_1$ -mediated stimuli in the large vessels outside the muscles, which ensured adequate peripheral transmission of a sufficient fraction of cardiac output; and (b) a mirror-like decrease in intramuscular TPVR due to inhibition of  $\alpha_2$  receptors, leading to a progressive drop in DABP while still ensuring nourishment of the muscles engaged in the escalating pedalling effort. Notably, in this subject, mean arterial blood pressure (MABP) remained at a good level despite the marked reduction in TPVR, with MABP around 90 Torr in both  $W_0$  and  $W_{\max}$  conditions. Furthermore, these adaptations provided a clear advantage for the heart mechanics, allowing it to deliver adequate oxygen to the working muscles at a lower energetic cost. Extending the observations from the reference cyclist to the seven athletes

tested—whose mean  $\pm$  SD values are reported in Table II—it is evident that the mean TFI, reflecting left ventricular preload impedance, reached a peak value at the end of the test that was not significantly different from the pre-test value. This finding indicates that, in all athletes, despite the progressive and substantial reduction in VET, preload continued to contribute to the volumetric component of stroke output until the conclusion of the test. Regarding the omeometric contributor index for stroke volume increase, namely the EVI, the peak increase observed in the graph of Figure 12 was approximately 154% of the resting value. This was lower than the mean peak value recorded across all tested subjects at  $W_{\max}$ , which reached +192%. However, since the peak EVI value of the reference athlete ( $3.07 \text{ } \Omega \cdot \text{s}^{-1}$ ) fell within the range of the standard deviation of the group mean (minimum SD from the mean =  $2.98 \text{ } \Omega \cdot \text{s}^{-1}$ ), it can reasonably be stated that the beat-to-beat pattern of EVI in the reference athlete can be considered representative of the mean behaviour observed across all participants. With respect to the peak values of the main bioimpedance-derived cardiodynamic variables—heart rate, stroke volume, and cardiac output—the percentage differences between the group mean and the representative subject were +10%, +5%, and +4%, respectively. As all three differences fall within the  $\pm$ SD calculated for each mean, it is reasonable to consider the workload-dependent cardiodynamic adjustments observed in the exemplar cyclist as representative of those occurring in the entire group of athletes studied.

## 6 CONCLUSIONS

In the competitive road cyclists tested in this study, cardiovascular adaptations similar to those observed in long-distance runners may have occurred, leading to improved exercise efficiency. In fact, their hearts appeared to function more efficiently by increasing stroke volume as workload rose, thereby delivering more oxygen to the working muscles at a relatively lower overall heart rate. These adaptations could be further supported by a possible increase in the capillary network of the leg muscles [44], as suggested by the marked decrease in mean value of TPVR observed during the test. This indicates that the amount of blood pumped per heartbeat increased, meaning that less pumping effort was required to circulate the same volume of blood—i.e., the mechanical efficiency of the heart was enhanced. Moreover, since in these cyclists the peak value of the left ventricular preload index (TFI) did not decrease compared with  $W_0$ , as previously reported in skilled long-distance runners after maximal treadmill exercise [45], this finding reinforces the conclusion that well-trained competitive road cyclists develop specific cardiovascular morpho-functional adaptations. These adaptations provide an advantage in maintaining high and prolonged levels of mechanically generated power at the pedals, primarily of aerobic origin, as also suggested by the high workload (77% of the peak value) at which their anaerobic threshold occurred during the exhaustive test.

## 7 STUDY LIMITATIONS

Unfortunately, this study is subject to several limitations. In particular, its small, all-male, single-session sample limits the generalizability of the findings. For these reasons, the present work should be regarded as a preliminary study. The authors are committed to collecting additional experimental data in the near future to address these limitations and thereby ensure the full applicability of the proposed method. Nevertheless, despite the restricted sample size and gender composition, the effect size statistics reported here provide substantial evidence of a robust physiological response to maximal exercise in this specific group of athletes.

## REFERENCES

- [1] Gardner A.S., Stephens S., Martin D.T., Lawton E., Lee H. and Jenkins D., Accuracy of SRM and power tap power monitoring systems for bicycling. *Med Sci Sports Exerc*, Vol. 36, No. 7, pp. 1252–1258, 2004.
- [2] Bouillod A., Soto-Romero G., Grappe F., Bertucci W., Brunet E. and Cassirame J., Caveats and recommendations to assess the validity and reliability of cycling power meters: A systematic scoping review. *Sensors*, Vol. 22, No. 1, pp. 386, 2022.
- [3] Belforte G., Bonisoli E., Eula G., Ivanov A. and Sirolli S., Design and Tests of Textile Pneumatic Muscles for Active Suits, *International Journal of Mechanics and Control*, Vol. 17, No. 01, pp. 37-48, 2016.
- [4] Belforte G., Raparelli T., Eula G., Sirolli S., Appendino S., Geminiani G.C., Geda E., Zettin M., Virgilio R. and Sacco K., Study and Realisation of a preliminary control system for the active exoskeleton called P.I.G.R.O., suitable for unloaded robotic neurorehabilitation treatments, *International Journal of Mechanics and Control*, Vol. 22, No. 01, pp. 125-142, 2021.
- [5] Garrosa M., Ceccarelli M. and V. Díaz, Biomechanics in vehicle accidents for risk analysis, *International Journal of Mechanics and Control*, Vol. 24, No. 01, pp. 43-52, 2023.
- [6] Shepertycky M., Burton S., Dickson A., Liu Y.F. and Li, Q., Removing energy with an exoskeleton reduces the metabolic cost of walking. *Science*, Vol. 80, No. 372, pp. 957–960, 2021.
- [7] Mohammadzadeh Gonabadi A., Pipinos I.I., Myers S.A. and Fallahtafi F., Optimizing hip exoskeleton assistance pattern based on machine learning and simulation algorithms: a personalized approach to metabolic cost reduction. *Front Robot AI*. Vol. 12, pp. 1669600, 2025.
- [8] Wu W.C., Concu A., Solinas R., Meloni L., Manuello-Bertetto A., Fois A., Loviselli A., Deledda A. and Velluzzi F., Metabolic power and energy cost of mechanical work carried out by a sailor engaged in a solo ocean race: a case study. *International Journal of Mechanics and Control*, Vol. 19, No. 02, pp. 19-32, 2018.
- [9] Garau M., Ruggiu M., Manuello M. and Concu A., Correlation between mechanical and metabolic energy during the gait cycle with and without jumping stilts. *International Journal of Mechanics and Control*, Vol. 19, No. 02, pp. 33-38, 2018.
- [10] Sheridan D., Jaspers A., Viet Cuong D., Op De Beéck T., Moyna N.M., de Beukelaar T.T. and Roantree M., Estimating oxygen uptake in simulated team sports using machine learning models and wearable sensor data: A pilot study. *PLoS One*, Vol. 20, No. 4, 2025.
- [11] Concu A. and Marcello C., Stroke volume response to progressive exercise in athletes engaged in different training modes. *Eur J Appl Physiol*, Vol. 66, pp. 11-17, 1993.
- [12] Kumari P.D., Singh K.M., Mayaluri Z.L., Sahoo P.K., Lenka S., Panda G. and Agir S.K., A hybrid variational mode decomposition framework for enhanced cardiac output estimation using impedance cardiography. *Sci Rep*, Vol. 15, No. 1, pp. 25784, 2025.
- [13] Marongiu E., Crisafulli A., Ghiani G., Olla S., Roberto S., Pinna M., Pusceddu M., Palazzolo M., Sanna I., Concu A. and Tocco F., Cardiovascular Responses during free-diving in the sea. *Int J Sports Med*, Vol. 36, pp. 297-301, 2015.
- [14] Campagna M., Lecca L.I., Velluzzi F., Serra C., Bianco P., Manuello Bertetto A., Dell’Osa A.H., Fanni B., De Pau A., Fois A., Melis L., Kalb A., Marcello R., Melis S., Concu A. and Tocco F., A mechatronic simulator of an aircraft cockpit to study, by a virtual flight test, cardiovascular fitness in airline pilots banned to fly since covid-19 lockdown. *International Journal of Mechanics and Control*, Vol. 23, No. 02, pp. 85-99, 2022.
- [15] Metshein M., Krivošei A., Abdullayev A., Annus P. and Märtens O., Non-Standard Electrode Placement Strategies for ECG Signal Acquisition. *Sensors (Basel)*, Vol. 22, No. 23, pp. 9351, 2022.
- [16] Tocco F., Mattana D.V., Solinas R., Velluzzi F., Usai P., Fois A., Melis L., Bianco P., Serra C., Manuello Bertetto A., Dell’Osa A.H., Pereira A.F., Cerina A., Loviselli L., Marcello R., Melis S. and Concu A., Cardiometabolic benefits from a coastal sailing in a radical cystectomy patient remotely controlled by an internet of thing mechatronic tool: a case study. *International Journal of Mechanics and Control*. Vol. 24, N. 02, pp. 39-61, 2023.
- [17] Tocco F., Solinas R., Velluzzi F., Massidda M., Mattana D.V., Fois A., Melis L., Manuello Bertetto A., Bonisoli E.†, Venturini S., Bianco P., Dell’Osa A.H., Pereira A.F., Melis S., Cerina A., Loviselli L., Marcello R. and Concu A., A mechatronic tool for revealing inverse relationships among heart’s stroke volume and head’s linear acceleration induced by moored boats rolling in elderly sailors with unchanged body sizes: a non-drug anti-hypertensive advantage?. *International Journal of Mechanics and Control*, Vol. 25, No. 01, pp. 133-142, 2024.
- [18] Dell’Osa A.H., Fois A., Cerina A., Pili F., Manuello Bertetto A., Velluzzi F., Bellomi G., Palmas M., Ruggiu M., Melis S., Tocco F., and Concu A., Impedance cardiography assessment during body immersion in a high concentrated water solution of magnesium chloride simulating space microgravity: a pilot study. *Journal of Physics: Conference Series*, Vol. 3014, pp. 012006, 2025.

- [19] Roux A., Optimal integration between mechanical and physiological quantities to maximize the performance of competitive cyclists. *Graduate thesis in Mechanical Engineering*, Referees: Proff. Manuello Bertetto A, Concu A, Politecnico di Torino, Italy, 2024.
- [20] Digo E., Ingrosso L., Vargas M., De Vito C. and Gastaldi C., A computational methodology for recumbent bicycle fitting to optimize aerodynamic efficiency while ensuring rider comfort. *International Journal of Mechanics and Control*, Vol. 25, No. 01, pp. 105-113, 2024.
- [21] Charvátová H, Procházka A. and Vyšata O., Motion assessment for accelerometric and heart rate cycling data analysis. *Sensors (Basel)*, 2020 Vol. 20, No. 5, pp.1523, 2020.
- [22] Salas-Montoro J.A., Valdivia-Fernández I., Rozas A., Reyes-Sánchez J.M., Zabala M. and Pérez-Díaz J.J., Do power meter data depend on the device on which they are collected? Comparison of eleven different recordings. *Sensors (Basel)*, Vol. 25. No. 2, pp. 295, 2025.
- [23] Tocco F., Crisafulli A., Marongiu E., Milia R., Kalb A. and Concu A., A portable device to assess underwater changes of cardiodynamic variables by impedance cardiography. *Journal of Physics: Conference Series*, Vol. 407, pp. 012026, 2012.
- [24] Bernstein D.P., A new stroke volume equation for thoracic electrical bioimpedance: theory and rationale. *Crit Care Med*, Vol. 14, No. 10, pp. 904-909, 1986.
- [25] Concu A., Respiratory and cardiac effect of passive limb movements in man. *Pflugers Arch Eur J Physiol*, Vol. 412, pp. 548-550, 1988.
- [26] Eeftinck Schattenkerk D.W., van Lieshout J.J., van den Meiracker A.H., Wesseling K.R., Blanc S., Wieling W., van Montfrans G.A., Settels J.J., Wesseling K.H. and Westerhof B.E., Nexfin noninvasive continuous blood pressure validated against Riva-Rocci/Korotkoff. *Am J Hypertens*, Vol. 22, No. 4, pp. 378-383, 2009.
- [27] Ruedisueli I., Ma J., Nguyen R., Lakhani K., Gornbein J. and Middlekauff H.R, Optimizing ECG lead selection for detection of prolongation of ventricular repolarization as measured by the Tpeak-end interval. *Ann Noninvasive Electrocardiol*, Vol. 27, No. 4, pp. e12958, 2022.
- [28] Eren-Zengin F., Tuncer D., Senaran H. and Uzer G., Effects of isolated gastrocnemius tightness on foot posture, strength, function, and balance in children aged 7-16: a case-control study. *BMC Sports Sci Med Rehabil*, Vol. 17, No. 1, pp. 289, 2025.
- [29] Pellegrino A., Toncelli L., Vanni S., Modesti A., Pedrizzetti G. and Modesti P.A., Structural and functional remodeling for elite cyclists during exercise; pressure-volume loops and hemodynamic forces analysis. *Am J Physiol Heart Circ Physiol*, Vol. 328, No. 3, pp. H393-H400, 2025.
- [30] Hoshi D., Fukuie M., Tomoto T., Qin W., Tarumi T., Sugawara J. and Watanabe K., Respiratory regulation and lung volume during aquatic and land-based exercise in healthy young adults. *Physiol Rep*, Vol. 13, No. 19, pp. e70564, 2025.
- [31] Sun X.G., Hansen J.E., Garatachea N., Storer T.W. and Wasserman K., Ventilatory efficiency during exercise in healthy subjects. *Am J Respir Crit Care Med*, Vol. 166, No. 11, pp. 1443-1448, 2002.
- [32] Sendra-Pérez C., Encarnacion-Martinez A., Salvador-Palmer R., Murias J.M. and Priego-Quesada J.I. Profiles of muscle-specific oxygenation responses and thresholds during graded cycling incremental test. *Eur J Appl Physiol*. Vol. 125, No. 1, pp. 237-245, 2025.
- [33] Milagro J., Hernández-Vicente A., Hernando D., Casajús J.A., Garatachea N., Bailón R. and Pueyo E., Estimation of the second ventilatory threshold through ventricular repolarization profile analysis. *Scand J Med Sci Sports*, Vol. 31, No. 2, pp. 339-349, 2021.
- [34] Libonati J.R., Myocardial diastolic function and exercise. *Med Sci Sports Exerc*, Vol. 31, No. 12, pp. 1741-1747, 1999.
- [35] George K., Oxborough D., Forster J., Whyte G., Shave R., Dawson E., Stephenson C., Dugdill L., Edwards B. and Gaze D., Mitral annular myocardial velocity assessment of segmental left ventricular diastolic function after prolonged exercise in humans. *J Physiol*, Vol. 15, No. 569(Pt 1), pp. 305-313, 2005.
- [36] Cheng, C.P., Igarashi Y. and Little W.C., Mechanism of augmented rate of left ventricular filling during exercise. *Circ Res*, Vol. 70, pp. 9-19, 1992.
- [37] Little, W.C. and Cheng C.P., Modulation of diastolic dysfunction in the intact heart. In : *Diastolic Relaxation of the Heart*, 2<sup>nd</sup> edition, B. H. Lorell and W. Grossman, Boston: Kluwer Academic Publishers, pp. 167-176, 1994.
- [38] Tate C.A., Taffet G.E., Hudson E.K., Blaylock S.L., McBride R.P. and Michael L.H., Enhanced calcium uptake of cardiac sarcoplasmic reticulum in exercise-trained rats. *Am J Physiol Heart Circ Physiol*, Vol. 258, No. 27, pp. H431-H435, 1990.
- [39] Katz A.M., *Physiology of the Heart*. New York: Raven Press, pp. 178-195, 1992.
- [40] Apstein C.S., Libonati J.R., Varma N., and Eberli F.R., *Exercise, Diastolic Function, and Dysfunction: Exercise and Heart Failure*, Eds. G. Balady and J. P. Armonk, NY: Futura Publishing, pp. 39-83, 1997.
- [41] Manuello Bertetto A., Tocco F., Bellomi G., Mulargia L., Ruggiu M., Palmas M., Massidda M., Ghiani G., Velluzzi F., Melis S., Fois A., Dell'Osa A.H., Cerina A., Bertelli U., Carta M.G., Bianco P.R. and Concu A., Cardiovascular and metabolic engagement after an endurance race in pilots driving motorboats electrically powered by green Energy. *International Journal of Mechanics and Control*, Vol. 26, No. 01, pp. 221-230, 2025.
- [42] Wray D.W., Fadel P.J., Smith M.L., Raven P. and Sander M., Inhibition of alpha-adrenergic vasoconstriction in exercising human thigh muscles. *J Physiol*, Vol. 555 No. 2, pp. 545-563, 2004.

- [43] Concu A., Cardiovascular adjustments during exercise: points and counterpoints, *New insight into cardiovascular apparatus during exercise*, Eds. Crisafulli A. and Concu A., Research Signpost, Kerala, India, pp. 61-84, 2007.
- [44] Saltin B., Kim C.K., Terrados N., Larsen H., Svedenhag J. and Rolf C.J., Morphology, enzyme activities and buffer capacity in leg muscles of Kenyan and Scandinavian runners. *Scand J Med Sci Sports*, Vol. 5, No. 4, pp. 222-230, 1995.
- [45] Percy R.F., Conetta D.A. and Miller A.B., Echocardiographic assessment of the left ventricle of endurance athletes just before and after exercise. *Am J Cardiol*, Vol. 65, No. 16, pp. 1140-1144, 1990.

